Chapter 2
X-Ray and Neutron Scattering Foundations for the Research in Antimicrobials

Daniel Piso

Abstract Scattering is becoming a very important alternative for research in biology. X-rays and neutrons permit to obtain information about the molecular processes, determine biological structures and even be helpful in the design of new drugs. Research in antimicrobials can also be benefited from instruments using these techniques. The history, physical foundations and theoretical apparatus that enable the extraction of information from scattering are explained. Big scientific facilities that play major role in scattering investigation are also mentioned. Some of them are already in operation, and others will provide the scientific community with powerful instruments in the short or medium term. Also, a basic description of the two most representative scattering techniques for biology is included. Finally, some success case of antimicrobials and biology investigations are included to illustrate the effectiveness of these experimental tools.

2.1 Introduction

During the last decades, neutron and X-ray scattering based techniques have become major alternatives in the research of static and dynamic biological structures. These techniques have proven to be two of the most powerful structural determination techniques, especially, for the study of membranes, which is one of the central axes in antimicrobials research.

The X-ray crystallography began when Max von Laue and his colleagues discovered that the phenomenon of interference of light could also be applied to X-rays. The distance between atoms in macromolecules is comparable to the radiation wavelength. This fact made von Laue come to the conclusion that a crystal would act as a three-dimensional interference lattice for X-ray radiation (Friedrich et al. 1912).

D. Piso (✉)
Control Division, European Spallation Source (ESS), Lund, Sweden
e-mail: daniel.pisofernandez@esss.se

T. G. Villa and P. Veiga-Crespo (eds.), *Antimicrobial Compounds*,
DOI: 10.1007/978-3-642-40444-3_2,

The next step was the determination of the structure of the compounds by using the information obtained from X-ray photographs. This accomplishment was done by Lawrence Bragg for the first time. What Lawrence Bragg did was to calculate the intensities of all reflections (interference points) in an X-ray diffraction photograph and to compare these values with the observed intensities. In 1915, W. L. Bragg and W. H. Bragg (son and father) shared the Nobel Prize in Physics, the son, W. L. Bragg, for his work on diffraction and crystal structures and his father, W. H. Bragg, for studies on the origin and properties of X-rays. Bragg's calculations were used by R. J. Havighurst to calculate the electron density distribution in a crystal of sodium chloride along cubic edges and cube diagonals (Havighurst 1927). Then, in 1934, J. D. Bernal published in Nature the photograph of a protein (pepsin) using X-ray crystallography (Bernal and Crowfoot 1934).

Particularly, X-ray crystallography has been successfully applied to solve the crystal structures of proteins, beginning in the late 1950s with the structure of the myoglobin and haemoglobin (Kendrew et al. 1958). From the calculated electron density maps, a model of the myoglobin molecule to 6 Å resolution was constructed. The model contained a number of dense rod-like features that had the dimensions of α-helices and made up the bulk of the polypeptide chain.

Early in the 1970s, Tardieu et al. (1973) published a study based on X-ray scattering describing the structure of a variety of lecithin-water phases observed below the "melting" temperature of the hydrocarbon chains. All the lamellar phases assumed by pure lipid/water systems were identified. The results emphasize the clear-cut difference between the liquid-like and the other types of partly ordered conformations, as well as the correlations which exist between the chemical composition and the structure of the lipids below the melting temperature of the chains. Since then, more than 60 K structures of proteins and other biological molecules have been determined with X-rays.

X-rays have wavelengths much shorter than the visible light, so they are useful to find atomic positions, mainly for crystalline materials. However, this technique is much more efficient when it comes to atoms with a high number of electrons. Because of that, the visibility for atoms involved in biological structures (oxygen and hydrogen) it is not so good. This is the main reason that led the scientist to consider neutrons to determine the matter structure.

Regarding neutrons, it was Ernest Rutherford who, in 1920, suggested that the difference between the atomic number and the atomic mass could be explained by the existence of a neutrally charged particle in the atomic nucleus (Rutherford 1920). Finally, James Chadwick proved the existence of the neutrons by analysing the radiation obtained when α particles fell on a beryllium layer (Chadwick 1932).

Neutrons have no charge and their electric dipole moment is almost zero, so they have a bigger penetration depth in matter. They interact with atoms via nuclear forces, which are very short range (10^{-15} m). So, the matter appears not very dense to neutrons and they can travel long distances through most materials without any interaction. For example, the attenuation of neutrons by aluminium is about 1 % per millimetre compared to 99 % in the case of X-rays.

Neutrons have a unique sensitivity to hydrogen atoms. This capability enables an accurate determination of molecular structures, which is important for the design of new therapeutic drugs. The bad part is that they are slightly scattered, and to obtain significant data, high flux of particles is needed. Because of this, they are more difficult to produce. In that sense, a big effort is being put in constructing high-performance facilities to obtain high-energy and flux neutron beams to operate different instruments that will be the most powerful ones to study a wide range of biological structures (Danared 2012; White 2002). There is also a great variety of instruments that make possible the extraction of useful information from different aspects of the neutron scattering.

The first neutron spectrometer was mounted at a port on the Oak Ridge graphite reactor in the mid-1940s. Most of the work with neutrons was focused on crystal lattices (Brockhouse and Hurst 1952). In 1955, Brockhouse and Stewart (Brockhouse and Stewart 1955) were the first people to observe the interaction of thermal neutrons with lattice phonons. Neutrons travelling through a crystal of aluminium both lost and gained energy through scattering. This changes in energy provided new information in interatomic forces and the normal modes of vibration.

The scattering of neutrons from hydrogen has driven an important experimental activity for the determination of the structure of biologically important compounds during the last decades. Biological experiments can be classified into two categories: high resolution and low resolution. The first technique determines the position of hydrogen atoms in biological molecules. The second one exploits the difference in sensitivity of neutron radiation to hydrogen and to deuterium in order to determine the location of molecular compounds in large structures.

Nowadays, there are big expectations when it comes to scattering techniques. Multiple applications that will help to understand the complexity of matter and nature are gathering big scientific efforts. A central part is the understanding of the molecular basis of the biological processes (Peggs 2013). Biological systems such as enzymes, tissues, organs rely on the interplay of large molecules such proteins and nucleic acids. Scattering methods are highly powerful probes for life sciences. The final goal is to decipher these molecular mechanisms through structural and dynamical analysis of complexes (Pieper et al. 2008; Wood et al. 2007). Antimicrobial research, as relying heavily in cell membrane structures and drug discovery, can also get benefit of scattering techniques, as shown later. Multiresistant bacterial strains threatening public health, individualized and preventive treatments approach are paradigmatic challenges to be addressed.

Even though there exist (especially in the X-ray world) some commercial instruments, the investigation that uses scattering is relying more and more in big facilities (accelerators). The second section of this chapter is devoted to accelerators: synchrotrons for producing X-rays and spallation sources for producing neutrons.

2.2 Accelerators

2.2.1 Synchrotrons and Storage Rings

Oliphant invented the synchrotron principle in 1943 (Oliphant 1943): *Particles should be constrained to move in a circle of constant radius thus enabling the use of an annular ring of magnetic field…, which would be varied in such a way that the radius of curvature remains constant as the particles gain energy through successive accelerations by an alternating electric field applied between coaxial hollow electrodes.*

By means of an injected short pulse, the field rises and the particles are accelerated until they have energy enough to hit a target or to be extracted out of the synchrotron. The particle acceleration is achieved by using fields in a RF resonator, fed by a radio transmitter. Particles return to the resonator at each turn of the synchrotron. The guiding field is provided by a ring of magnets.

Later on, Veksler (1944) and McMillan (1945) completed the concept by means of the *Phase Stability Principle*. If the particles are arranged to ride in the rising edge of the field wave in the accelerator cavity, they receive more energy when they are late and less energy when they are early. So, the particles end up oscillating about the stable synchronous phase.

The synchrotron acceleration was demonstrated by first time in 1946 by Goward and Barnes (Goward and Barnes 1946) in a refurbished machine at Woolwich Arsenal, UK. Only 2 months later, Elder et al. (1947) operated a 70 MeV machine built by them at General Electrics Laboratories in USA.

The acceleration of particles to very high speeds in synchrotrons produces radiation. Particularly, this is the technique used in accelerators to produce X-rays. The speed of particles in synchrotrons is highly relativistic, and the power radiated is proportional to the fourth power of the particle speed and is inversely proportional to the square of the radius of the path. It becomes the limiting factor on the final energy of particles accelerated in electron synchrotrons:

$$P \approx \frac{2\mathrm{K}e^2\gamma^4 v^4}{3c^2 r^2}. \tag{2.1}$$

For an accelerator like a synchrotron, the radius is fixed after construction, but the inverse dependence of synchrotron radiation loss on radius argues for building the accelerator as large as possible.

Nowadays, more than 50 synchrotron light sources big facilities exist in the world (Lightsources). Here, in Table 2.1, some of the more outstanding installations are summarized. All of them operate accelerating particles at high energies in very big rings. Almost any of these facilities are putting big effort in the investigation in structural biology and new drugs design as we will show later.

Table 2.1 Example of facilities using high-energy synchrotrons

Name	Accelerator energy (GeV)	Ring diameter (m)
Diamond light source (Suller 2002)	3	561
ESRF (Revol et al. 2013)	6	844
APS (Borland et al. 2007)	7	1104
MAX IV (Curbis et al. 2013)	3	528

2.2.2 Spallation Sources

As mentioned before, high flux of neutrons is required to keep on developing more and more advanced instruments for neutron science. This can be achieved by using spallation sources. They produce neutrons by means of the interaction of high-energy protons (GeV) with a heavy metal target (Broome 1996) (Fig. 2.1).

The protons interact with the target, and a few energetic particles are produced. The nucleus transitions to a highly excited state. While it comes back to the ground state, it emits neutrons, protons, deuterons, tritons and alpha particles (evaporation). The energetic particles go on to interact with other target nuclei producing more excited nuclei and more neutrons in a nuclear cascade.

For some materials, the excited nuclei will undergo fission to leave two fragments which will come to ground state by evaporation. All these processes generate a lot of heat in the target, and it has to be refrigerated.

The energy of neutrons suitable for scattering ranges from neV to eV. The number of produced neutrons depends on the proton energy. Neutron scattering is an intensity limited field because its interaction with the matter is weak. Because of this, there is a strong interest in more powerful neutron sources. Table 2.2 shows the evolution of the main characteristics of neutron sources. The upper facilities were the first neutron sources designed. Meanwhile, the last one (ESS) is

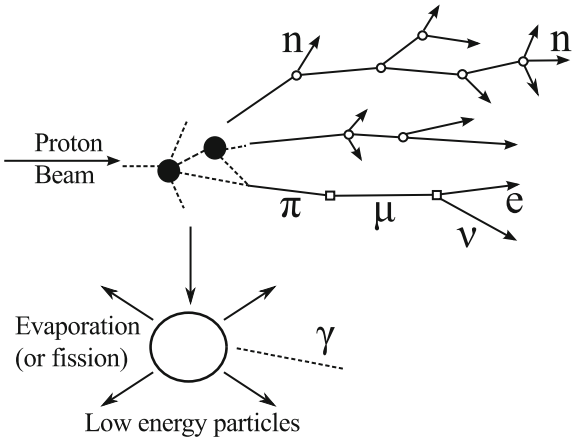

Fig. 2.1 The spallation process

Table 2.2 Main parameters of different facilities producing neutrons

Name	Accelerator energy	Average beam power (MW)	Repetition rate (HZ)	Protons per pulse (10^{13})	Pulse length at target (μs)
IPS, ANL (Brow 1995)	50 meV Linac 500 meV RCS	0.0075	30	0.3	0.1
ISIS, RAL (Gardner 1994)	70 meV Linac 800 meV RCS	0.16	50	2.5	0.45
SINQ, PSI (Bauer et al. 1997)	590 meV Cyclotron	$\leq$0.9	C. W.	–	–
LANSCE, LANL (Garnett et al. 2011)	800 meV	1	30	–	1,200
SNS, ORNL (Plum 2010)	2.5 GeV	1.4	60	15	1,000
ESS (Eshraqi and Danared 2011)	2.5 GeV	5	14	9.10^5	2.87

still to be constructed in the following months. The energy delivered and the number of protons produced is much bigger nowadays, which severely affects to the neutrons production rates.

2.3 Foundations of X-ray Scattering

The interatomic distances in crystals and molecules amount to 0.15–0.4 nm which correspond to the wavelength of the electromagnetic spectrum for X-rays having photon energies between 3 and 8 keV. Accordingly, phenomena like constructive and destructive interference should become observable when crystalline and molecular structures are exposed to X-rays.

There are three types of interactions when a sample is illuminated with X-rays (Cullity 1967; Warren 1969):

- Electrons may be liberated from their bound atomic states in the process of photoionization. This is an inelastic scattering process.
- A second type of inelastic scattering is the so-called Compton scattering. Energy is transferred to an electron, which proceeds, however, without releasing the electron from the atom.
- Finally, X-rays may be scattered elastically by electrons (Thomson scattering). The electron oscillates as a dipole at the frequency of the incoming beam and becomes a source of radiation. The wavelength λ of X-rays is conserved for Thomson scattering. This is the process used for structural investigations by X-ray diffraction.

Figure 2.2 shows elastic scattering for a single free electron of charge e, mass m and at position R_0. The incoming beam is accounted for by a plane wave:

$$E_0 \cdot \mathrm{e}^{-i\left(\vec{K}_0 \cdot \vec{R}_0\right)}. \tag{2.2}$$

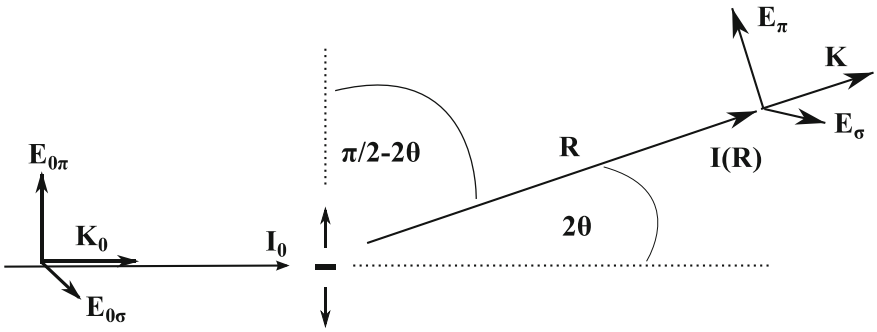

Fig. 2.2 Single electron scattering centre

E_0 is the electrical field vector and K_0 the wave vector.

The dependence of the field on time will be neglected throughout. The wave vectors K_0 and K describe the direction of the incoming and exiting beam and both are of magnitude $2\pi/\lambda$. The plane defined by them is denoted as the scattering plane. The angle between K and the prolonged direction of K_0 is the scattering angle that will be denoted by 2θ:

$$2\theta = \arccos \frac{\langle \vec{K},\, \vec{K}_0 \rangle}{K \cdot K_0}. \tag{2.3}$$

The oscillating charge e will emit radiation of the same wavelength λ as the primary beam. If the amplitude of the scattered wave $E(R)$ is considered at a distance R, the mathematical expression is

$$E(R) = E_0 \frac{1}{4\pi\varepsilon_0 R} \frac{\mathrm{e}^2}{\mathrm{mc}^2} \sin \angle(E_0,\, R) \mathrm{e}^{-\mathrm{i}\vec{K}\cdot\vec{\mathrm{R}}}. \tag{2.4}$$

where ε_0 and c are the vacuum permittivity and velocity of light. The field vector E and wave vector K are oriented perpendicular to each other as is usual for electromagnetic waves. The field vectors in both cases will be denoted by $E\pi$ and $E\sigma$. The angle between $E\sigma$ and R is always 90°, and the sin term will equal unity. For the case of π polarization, however, it may be expressed by virtue of the scattering angle according to $\sin \angle(E_0, R) = |\cos\, 2\theta|$. Since the intensity is obtained from the sum of the square of both field vectors, the expression

$$\left(\frac{1}{4\pi\varepsilon_0}\right)^2 \left(\frac{\mathrm{e}^2}{\mathrm{mc}^2}\right) \left(\mathrm{E}_\sigma^2 + \mathrm{E}_\pi^2 \cos^2 2\theta\right) \tag{2.5}$$

in a non-polarized beam both polarization states will have the same probability of occurring

$$\bar{E}_\sigma^2 = \bar{E}_\pi^2 = \frac{I_0}{2}. \tag{2.6}$$

Then, the intensity of the scattered beam at distance R is finally obtained:

$$I(R) = I_0 \frac{r_e^2}{R^2} \frac{1 + \cos^2 2\theta}{2}. \tag{2.7}$$

The intensity of the scattering scales with the inverse of R^2 and r_e^2. For distances R of the order of 10^{-1} m, the probability of observing the scattering by a single electron tends to zero. In this analysis, only the scattering from electrons is taken into account. From Eq. (2.5), it can also be derived that the interaction for atomic nuclei is 10^{-6} times smaller and then neglectable. Therefore, from the point of view of scattering, the atoms are modelled by the number of electrons within them. r_e is substituted by Zr_e (Z is the number of electrons) in this development to reach a quantitative description for the X-ray elastic scattering from an atom.

Atomic positions are described by the lattice vector $r_{n_1,n_2,n_3} = n_1 a c_1 + n_2 a c_2 + n_3 a c_3$ with c_1, c_2 and c_3 being the unit vectors of the three orthogonal directions in space. The task is to quantify the strength of the scattered fields at a point R when elastic scattering occurs according to Eq. (2.4) at all atoms. The reference point of R is chosen such that it starts at the origin of the crystal lattice r_{000}. The wave vector of the primary beam K_0 is assumed to be parallel to the [100] direction of the crystal. The scattering plane defined by K_0 and K may coincide with one of the (010) planes. The wavefronts of the incoming plane waves, which are the planes of constant phase, are then oriented parallel to (100) planes. An atom on the position r_{n_1,n_2,n_3} would then cause a scattering intensity to be measured at R (assuming $r_{n_1,n_2,n_3} \ll R$—Fraunhofer diffraction)

$$E_0 \frac{Zr_e}{R} e^{-iKR} \sum_{n_1,n_2,n_3} e^{-i(K-\vec{K}_0) r_{n_1,n_2,n_3}}. \tag{2.8}$$

The strength of the total scattered field depends on the spatial orientation of the wave vectors K_0 and K with respect to the crystal reference frame $\{c_i\}$.

The quantity $Q = K - K_0$ is called the *scattering vector*.

The geometric construction of vector Q in Fig. 2.3 shows that the scattering vector magnitude is

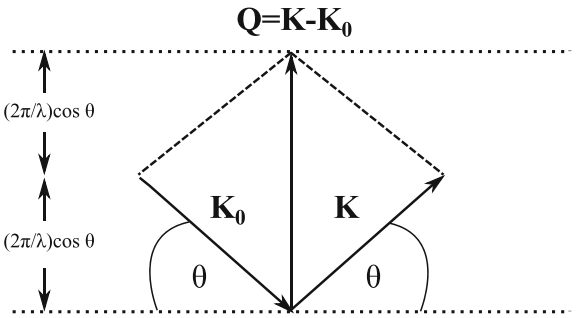

Fig. 2.3 Scattering vector geometry

$$|Q| = \frac{4\pi}{\lambda} \sin\theta. \tag{2.9}$$

The scattering vector Q is a physical quantity fully under the control of the experimentalist. The orientation of the incident beam (K_0) and the position of the detector (K) decide the direction in which the scattering vector (Q) of X-rays proceeds. And the choice of wavelength determines the amplitude transfer to which the sample is subjected. From these considerations, it is possible to understand the collection of a diffraction pattern as a way of scanning the sample's structure by scattering vector variation.

If the summation factor of Eq. (2.8) is expanded into three individual terms and the geometry of the simple lattice is used, it is found that the field amplitude of the scattered beam is proportional to

$$\sum_{n_1=0}^{N_1-1} \sum_{n_2=0}^{N_2-1} \sum_{n_3=0}^{N_3-1} \mathrm{e}^{-iQ(n_1ac_1+n_2ac_2+n_3ac_3)}. \tag{2.10}$$

From this equation, it is possible to reach the interference function. It describes the distribution of scattered intensity in the space around the crystal.

$$\Im(Q) = \frac{\sin^2(N_1aQc_1/2)}{\sin^2(aQc_1/2)} \frac{\sin^2(N_2aQc_2/2)}{\sin^2(aQc_2/2)} \frac{\sin^2(N_3aQc_3/2)}{\sin^2(aQc_3/2)}. \tag{2.11}$$

For large values of $N1$, $N2$ and $N3$, the three factors in $\Im$(Q) only differ from zero if the arguments in the $\sin^2$ function of the denominator become integer multiples of π. Let us name these integers h, k and l in the following:

$$\Im(Q) \to \max \Leftrightarrow aQc_1 = 2\pi h,\ aQc_2 = 2\pi k,\ aQc_3 = 2\pi l. \tag{2.12}$$

This equation yields as condition for maximum intensity

$$I(R) \to \max \Leftrightarrow \frac{|Q|}{2\pi} = \frac{\sqrt{h^2+k^2+l^2}}{a} \tag{2.13}$$

which can be rewritten by inserting the magnitude of the scattering vector (Eq. 2.9).

$$I(R) \to \max \Leftrightarrow 2\frac{a}{\sqrt{h^2+k^2+l^2}} \sin\theta \tag{2.14}$$

The distance between two adjacent planes is called the *interplanar spacing*

$$d_{hkl} = \frac{a}{\sqrt{h^2+k^2+l^2}} \tag{2.15}$$

Keeping this meaning of integer triples in mind, Eq. (2.14) tells us that to observe the maximum intensity in the diffraction pattern of a simple cubic crystal, and the following equation must be satisfied:

$$2d_{hkl} \sin\theta = n\lambda. \tag{2.16}$$

The equation is called *Bragg equation* and was applied by W.H. Bragg and W.L. Bragg in 1913 to describe the position of X-ray scattering peaks in angular space.

A sample with crystallographic lattice planes with distances d_{hkl} is irradiated by plane wave X-rays impinging on the lattice planes at an angle θ. The relative phase shift of the wave depends on the configuration of atoms.

Having arrived at this point, it can be stated that we have identified the positions in space where constructive interference for the scattering of X-rays at a crystal lattice may be observed. It has been shown that measurable intensities only occur for certain orientations of the vector of momentum transfer Q with respect to the crystal coordinate system $\{c_i\}$. Various assumptions were made that were rather crude when the course of the intensity of Bragg reflections is of interest. It has been assumed, for instance, that the atom's electrons are confined to the centre of mass of the atom. In addition, thermal vibrations, absorption by the specimen, etc., were neglected.

2.4 Foundations of Neutron Scattering

The best way of understanding neutron scattering is looking at how a neutron is scattered by a single nucleus. Then, if the effects of different nuclei are accounted, it is possible to describe phenomena like neutron diffraction, inelastic neutron scattering, etc. The physics of neutron scattering is a quantum mechanical process (Liang et al. 2009). Therefore, it is necessary to bear in mind the wave-particle duality to understand its fundamentals. Essentially, this means that the square modules of the wave function of a neutrons gives the probability of finding that neutron in a particular point in space.

The speed of neutrons and their wavelength are inversely proportional. Normally, a wave vector $\vec{k}$ pointing along the neutrons' trajectory is defined as having magnitude $2\pi/\lambda$. It can also be related to the neutron velocity through the equation.

$$\left|\vec{k}\right| = 2\pi m v/h \tag{2.17}$$

h is the Planck's constant, and m is the neutron's mass.

If a neutron passes close to a nucleus within an effective area, called *cross section* σ, it is scattered in any direction with equal probability (Fig. 2.4).

This scattering is isotropic because the range of the nuclear interaction between the neutron and the nucleus is tiny compared to the wavelength of the neutron. As shown in Fig. 2.4, the wave of an incident neutron is represented as a plane wave $\left(e^{ik\cdot x}\right)$, without loss of generality. Additionally, the modulus of this wave is 1, so

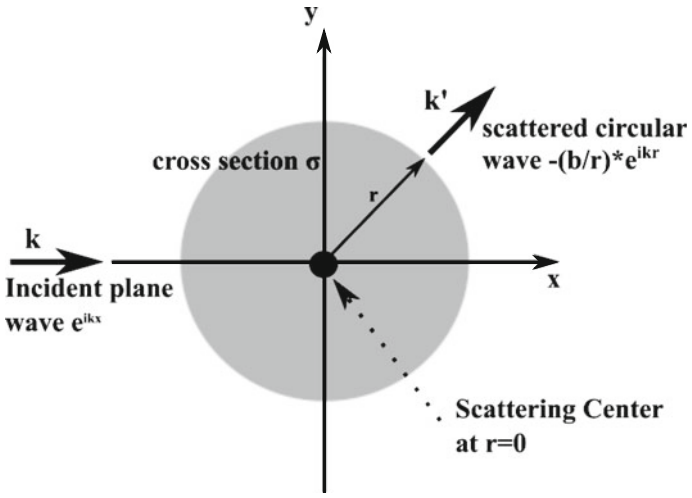

Fig. 2.4 Single neutron scattering centre

the probability of being found anywhere is the same but has a definite momentum $mv = h\upsilon/2\pi$.

The wave of the scattered neutrons depends on the interaction between the neutron and the nucleus. When the nucleus is considered to be at the origin of the coordinate system, the wave of the scattered neutron is $-(b/r) \cdot e^{ik \cdot r}$ and it is a circular wave. The square of this function gives the intensity of the neutron beam, which decreases with the term $1/r^2$. b gives the strength of the interaction between the nucleus and the proton (*scattering length*). And the minus means for repulsive interaction.

The strength of the interaction is not directly related with the atomic number (Diagnoux and Lander 2003). For example, hydrogen and deuterium, which are very important in the study of biological structures, have scattering lengths that are relatively large and very different from each other. This difference is used to label biological molecules with different isotopes in such a way that boosts the amount of information obtained from neutron scattering experiments.

To reproduce how matter scatters neutrons, the addition of the contribution of all individual scattering centres has to be performed. Regardless of the type of collision (elastic or inelastic), the energy and momentum are conserved. If the neutron losses energy E, the same amount is gained by the scattering nucleus.

From Eq. (2.17), it could be easily derived the momentum lost by the neutron in the collision (*momentum transfer*).

$$m \cdot \Delta\vec{v} = \frac{h}{2\pi}\vec{Q} = \frac{h}{2\pi}(\vec{k} - \vec{k}') \tag{2.18}$$

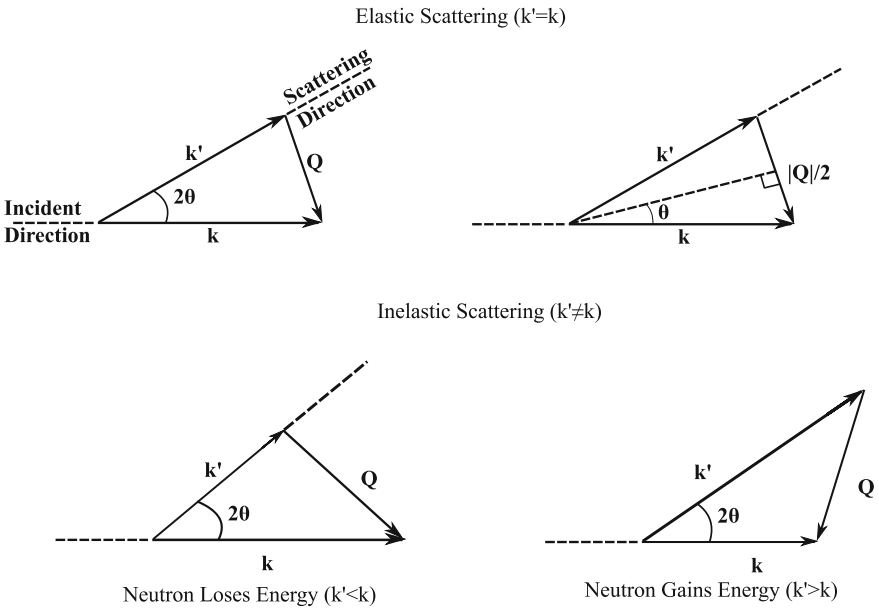

Fig. 2.5 Scattering triangles for elastic and inelastic scattering

(see also Fig. 2.5) $\vec{k}$ is the wavevector of the incident neutron and $\vec{k}'$ of the scattered one. $\vec{Q}$ is called the *scattering vector*. Finally, the angle 2θ is the angle between the trajectory of the incident neutron and the scattered one (*scattering angle*).

In the case of the elastic scattering ($\left|\vec{\mathrm{k}}\right| = \left|\vec{\mathrm{k}}'\right|$), with simple trigonometric rules, we can obtain:

$$\sin\theta = \frac{Q/2}{K} \tag{2.19}$$

and then,

$$Q = 2 \cdot \mathrm{k} \cdot \sin\theta = \frac{4 \cdot \pi \cdot \sin\theta}{\lambda} \tag{2.20}$$

For all neutron experiments, the most important magnitude is the intensity of neutrons as a function of the scattering vector $\vec{Q}$ and the energy E, $I(\vec{Q}, E)$.

Van Hove showed in 1954 (van Hove 1954) that the intensity of neutrons can be written in terms of time-dependent correlations between the positions of pair of scattering atoms. This result is crucial for the scattering problem because it permits to represent the intensity as proportional to a Fourier transform, which gives the probability of finding two atoms separated by a certain distance. This is the key, because if the intensity of neutrons is known, it is possible to derive the atoms positions in the sample and, hence, the sample structure.

The probability of a neutron with wavevector $\vec{k}$ being scattered by a potential $V(\vec{r})$ and becoming a new outgoing wavevector $\vec{k}'$ (Born approximation (Gottfried and Yan 2003)) is proportional to the module of the following probability function:

$$\left| \int \mathrm{e}^{i\vec{k}\vec{r}} V(\vec{r}) \mathrm{e}^{i\vec{k}'\vec{r}'} d\vec{r} \right|^2 = \left| \int \mathrm{e}^{ik\vec{Q}\vec{r}} V(\vec{r}) d\vec{r} \right|^2 \tag{2.21}$$

This probability is integrated over the whole sample. $V(\vec{r})$ is the so-called *Fermi pseudo-potential*, which for an assembly of nuclei situated at positions $\vec{r}_j$ is given by

$$V(\vec{r}) = \frac{2\pi\hbar}{m} \sum_j b_j \delta(\vec{r} - \vec{r}_j) \tag{2.22}$$

m is the neutron's mass. $\delta(\vec{r})$ is a Dirac delta that takes unity value at the atoms positions. b_j is the scattering length mentioned before. Taking all this into account, the scattering law $I(\vec{Q}, E)$ can be written as (Squires 2012):

$$I(\vec{Q}, E) = \frac{1}{h} \frac{k'}{k} \sum_{i,j} b_i b_j \int_{-\infty}^{\infty} \left\langle \mathrm{e}^{-i\vec{Q}\cdot\vec{r}_i(0)} \mathrm{e}^{-i\vec{Q}\cdot\vec{r}_j(t)} \right\rangle \mathrm{e}^{-i(E/\hbar)t} dt. \tag{2.23}$$

Equation (2.23) is a sum over all of the positions of the nuclei in the sample. The angular brackets indicate that a thermodynamic average over all possible configurations of the sample is needed. In order to better understand the physical meaning of these mathematical expressions, it is possible to simplify (2.23) treating vectors as classical (not quantum mechanical) quantities:

$$\sum_{i,j} b_i b_j \left\langle \mathrm{e}^{-i\vec{Q}\{\vec{r}_i(0) - \vec{r}_j(t)\}} \right\rangle = \sum_{i,j} b_i b_j \int_{\text{sample}} \delta(\vec{r} - \vec{r}_i(0) + \vec{r}_j(t)) \, \mathrm{e}^{-i\vec{Q}\cdot\vec{r}} d\vec{r} \tag{2.24}$$

Another useful simplification is to assume that in the sample, all the nuclei have the same scattering length $b_i = b_j = b$. The right hand of the previous equation becomes

$$\mathrm{N}b^2 \int_{\text{sample}} G(\vec{r}, t) \mathrm{e}^{-i\vec{Q}\cdot\vec{r}} \tag{2.25}$$

where

$$G(\vec{r}, t) = \frac{1}{N} \sum_{i,j} \delta(\vec{r} - [\vec{r}_i(0) - \vec{r}_j(t)]) \tag{2.26}$$

N is the number of nuclei in the simple. $G(\vec{r}, t)$ is the so-called the *time-dependent pair correlation function*, which describes how the correlation between the positions of nuclei evolves with time.

Finally, the Van Hove's scattering law is proportional to the space and time Fourier transforms of the time-dependent correlation function. Inverting Eq. (2.26), we can obtain information of the sample structure from neutron scattering information.

However, generally the scattering lengths are not the same. Even if a sample for the same isotope is considered, the interaction between the matter and the neutron depends on the spin state. Conversely, it is possible to average them over all spin states. The average interaction is denoted by angular brackets:

$$\sum_{i,j} \langle b_i b_j \rangle A_{ij} = \sum_{i,j} \langle b \rangle^2 A_{ij} + \sum_i \left(\langle b^2 \rangle - \langle b \rangle^2 \right) A_{ij} \tag{2.27}$$

A_{ij} is the integral in Eq. (2.26).

The first term in (2.27) is *coherent scattering* and depends on the distance between nuclei. The *elastic coherent scattering* produces information about the equilibrium structure, and *inelastic coherent scattering* produces information about the collective motion of the atoms.

The second term is the *incoherent scattering* and is the same for all atoms, independently of others. *Incoherent elastic scattering* does not provide useful information and is considered as undesired background in neutron scattering experiments. *Incoherent inelastic scattering* provides information about atomic diffusion.

2.5 Two Important Scattering Techniques for Antimicrobial Research

X-rays and neutrons have properties of plane waves, that is, amplitude and wavelength, and as they pass through matter, secondary wavelets are generated by interactions with individual atoms, and the resulting coherent scattering can constructively or destructively interfere.

Small-angle scattering arises from these coherent secondary wavelets that are scattered by atoms within a single molecule, and as a result, it is observed for molecules in crystals or in solution. This is a very useful technique, and it is considered the most important application for the study of biological macromolecules. It is able to characterize the shapes and dispositions of components within bimolecular complexes.

Although small-angle scattering solution is often described as a low-resolution technique (as it does not provide information on atomic coordinates), it is more appropriate to describe it as a technique capable of providing high-precision information with respect to size and shape. It is the rotational averaging of the molecules in solution that limits the information content of small-angle scattering more than the resolution limits of the experiments.

To interpret scattering data in terms of accurate structural parameters, the scattering signal must be measured from a sample of monodisperse, identical particles. Sample preparation is therefore a critically important.

A highly collimated X-ray or neutron beam is used to illuminate the sample, usually a protein or macromolecular complex in solution (typically >1 mg m L^{-1} in 5–30 μL for X-ray scattering and >3 mg m L^{-1} in 150–300 μL for neutron scattering). Traditionally, the radiation is of a single wavelength (or narrow band of wavelengths), although the development of pulsed neutron sources has led to time-of-flight neutron scattering instruments that can use white radiation to maximize flux. The scattered radiation is recorded on a detector, while the direct beam is usually absorbed by a beam stop; the size and position of which are key factors determining the minimum angle measured in an experiment. New developments in solid-state devices have led to detectors that can absorb an intense direct X-ray beam without incurring damage.

2.5.1 Small-Angle X-ray Scattering

Small-angle X-ray scattering (SAXS) is a fundamental method for structure analysis of condensed matter. The applications cover various fields, from metal alloys to synthetic polymers in solution and in bulk, biological macromolecules in solution, emulsions, porous materials, nanoparticles, etc. First X-ray applications date back to the late 1930s when the main principles of SAXS were developed in the seminal work of Guinier and Fournet (1955). This technique provides structural information on inhomogeneities of the electron density with characteristic dimensions between one and a few hundred nm.

The colloidal dimensions (tens or thousands of Å) are very large compared to X-rays wavelength. This fact makes the scattering angle very small when a sample is illuminated. So, X-ray scattering is only observed when there are electron density inhomogeneities of colloidal size in the sample. That means that this technique is not able to reveal the atomic structure of the materials. However, it is able to measure the shapes and sizes of nanoparticles and large molecules.

SAXS works in liquids or solids and has short response times, so it can be used to follow biological processes in real time. This makes SAXS an ideal complement to time-consuming analytical techniques such as electron microscopy and X-ray diffraction.

In particular, if a usual wavelength of 1 Å is used, the scattering radiation pattern is limited to a scattering angle of one or two degrees. In general, there are two restrictions that simplify this technique significantly: the system is statistically isotropic and there is no correlation between point separated wide enough. Then, the radiation pattern (of an electron density distribution $\bar{\rho}^2$) depends only on the

distance (r). Any phase factor e^{-ihr} of an incident plane wave can be replaced by its average over all r directions.

$$\left\langle e^{-ihr} \right\rangle = \frac{\sin hr}{hr}. \tag{2.28}$$

Then, the intensity is reduced to

$$I(h) = \int_0^\infty 4\pi r^2 \bar{\rho}^2(r) \frac{\sin hr}{hr} dr. \tag{2.29}$$

At large r, the respective electron densities should become independent and might be replaced by the mean value of ρ. In this case, for extremely small angles, the constant value across the whole volume acts like a blank object. Therefore, it makes no contribution to the diffraction pattern. It is then convenient to drop this background from the beginning.

The simplest case is that particles show spherical symmetry. As all orientations in space are equivalent, considering an sphere of radius R_0 and volume V of uniform density, we obtain

$$I_s(h) = (\Delta\rho)^2 V^2 \left[3 \frac{\sin hR_0 - hR_0 \cos hR_0}{(hR_0)^3} \right]^2 \tag{2.30}$$

For particles of non-spherical shape, the intensity can only be calculated by numerical methods. If we consider some symmetry orientation and we expand the expression for intensity in a power series, we obtain the Guinier approximation, which is a universal approximation for all particles.

$$I(h) = I(0) e^{-\frac{h^2 R^2}{3}} \tag{2.31}$$

R is the only parameter of this equation and is called *radius of gyration*. This Guinier formula holds incredibly well in the majority of the cases. Only in very anisometric particles, it should be replaced by another approximation.

High concentration of inhomogeneities reduces the intensity at low scattering angles. There are well-developed commercial instruments providing this technique. But if higher intensities are required, there exist highly specialized and powerful instruments (radiation from synchrotrons), as mentioned before. All modern synchrotrons provide SAXS beamlines. These instruments offer the possibility of performing time-resolving studies or observation of transient states in macromolecular assemblies. Moreover, in many problems, particularly the determination of density inhomogeneities within a particle, neutron techniques are the only solution.

2.5.2 Small-Angle Neutron Scattering

The theoretical apparatus used for small-angle neutron scattering (SANS) is very similar to that developed for X-rays. We have seen already in our discussion of diffraction that elastic scattering at a scattering vector $Q = (4\pi/\lambda)\sin\theta$ results from periodic modulations of the neutron scattering lengths with period $d = 2\pi/Q$. Combining these two expressions gives us Bragg's Law (Eq. 2.16). In the case of a crystal, d was interpreted as the distance between planes of atoms. To measure structures that are larger than typical interatomic distances, we need to arrange for Q to be small, either by increasing the neutron wavelength, λ, or by decreasing the scattering angle. Because it is not know how to produce very high fluxes of very long wavelength neutrons, it is always needed to use small scattering angles to examine larger structures such as polymers, colloids, or viruses. For this reason, the technique is known as small-angle neutron scattering, or SANS.

For SANS, the scattering wavevector, Q, is small, so the phase factors in do not vary greatly from one nucleus to its neighbour. For this reason, the sum in Eq. (2.23) can be replaced by an integral, and the intensity for SANS can be written as

$$S(\vec{Q}) = \left| \int_{\text{sample}} \rho(\vec{r}) \mathrm{e}^{i\vec{Q}\cdot\vec{r}} d\vec{r} \right|^2 \tag{2.32}$$

where $\rho(\vec{r})$ is a spatially varying quantity called the *scattering length density* calculated by summing the coherent scattering lengths of all atoms over a small volume (such as that of a single molecule) and dividing by that volume. In many cases, samples measured by SANS can be thought of as particles with a constant scattering length density, ρ, that are dispersed in a uniform medium with scattering length density ρ_m. Examples include pores in rock, colloidal dispersions, biological macromolecules in water and many more. The integral in Eq. (2.32) can, in this case, be separated into a uniform integral over the whole sample and terms that depend on the difference, $(\rho_p - \rho_m)$, a quantity often called the contrast factor. If all of the particles are identical and their positions are uncorrelated, Eq. (2.32) becomes

$$S(\vec{Q}) = N(\rho_p - \rho_m)^2 \left| \int_{\text{sample}} \rho(\vec{r}) \mathrm{e}^{i\vec{Q}\cdot\vec{r}} d\vec{r} \right|^2 \tag{2.33}$$

where the integral is now over the volume of one of the particles, and N_p is the number of particles in the sample. The integral of the phase factor $\mathrm{e}^{-i\vec{Q}\cdot\vec{r}}$ over a particle is called the form factor for that particle. For many simple particle shapes, the form factor can be evaluated analytically, whereas for complex biomolecules, for example, it has to be computed numerically.

Usually, the intensity one sees plotted for SANS is normalized to the sample volume so that $S(Q)$ is reported in units of cm^{-1} (as compared with Eq. (2.33), which has units of length squared).

Equation (2.33) allows us to understand an important technique used in SANS called contrast matching. The total scattering is proportional to the square of the scattering contrast between the particle and the matrix in which it is embedded. If we embed the particle in a medium whose scattering length density is equal to that of the particle, the latter will not scatter—it will be invisible.

The form factor in Eq. (2.33) will be evaluated by integrating over this central region only. The scattering patterns will be different in the external and central regions, and from two experiments, we will discover the structure of both the coating and the core of the particle. Variation of the scattering length density of the matrix is often achieved by choosing a matrix that contains hydrogen (such as water). By replacing different fractions of the hydrogen with deuterium atoms, a large range of scattering length densities can be achieved for the matrix. Both DNA and typical proteins can be contrast matched by water containing different fractions of deuterium. Isotopic labelling of this type can also be applied to parts of molecules in order to highlight them for neutron scattering experiments.

2.6 Antimicrobial and Biological Research Using Scattering

One of the major troubles in the design of new antimicrobials is how to attack the lipid bilayer of cell membranes. Some antimicrobial peptides exert their activity directly in the plasmatic membrane but the question is, how? Antimicrobial peptides secretion is a part of a natural immune response of many living organisms, acting as a rapid response to infection by diverse bacterial species, attacking directly the lipid bilayer or across a receptor (Latal et al. 1997; Lohner and Prenner 1999).

He and co-workers (He et al. 1995) were able to describe how alamethicin, an antimicrobial peptide, was able to create aqueous pores in the cell layer using the neutron in-plane scattering. Also, they were able to determinate that the pore formation was concentration-dependent process and a critical lipid value had to be reached to form a 18 Å in diameter pore. This pore formation was the molecular mechanism of the antimicrobial action. Thanks to this technique, it was possible, also, to determine the water dependence of the process (He et al. 1996). Similar research was done to determinate the pore structure originated by magainin (Ludtke et al. 1996).

The antimicrobial peptide protegrin-1 (PG-1) interacts with membranes in a manner that strongly depends on membrane composition: different lipids, different speed of integration in the lipid matrix. This integration is responsible of the cell membrane destabilization and, consequently, the cell death. In the case of the gram-negative bacteria, the integration occurs primary in the outer membrane

of the cell wall, thus allowing the AMP to reach the inner membrane. Thanks to X-ray scattering technique, it was possible to differentiate how PG-1 interact different kind of lipid bilayers (Gidalevitz et al. 2003).

The lipid A is one of the major components of the outer membrane of gram-negative bacteria. The X-ray scattering techniques of X-ray reflectivity (XR and grazing incident X-ray diffraction coupled to pressure-area isotherm methods were crucial to elucidate the disposition of these lipids in the outer membrane of bacteria at the level of air–aqueous interface (Neville et al. 2006). The analysis let also determinate that the hydrocarbon-associated chains are responsible of rigidity.

Not only the structure of the new potential drugs is important, but also it is mandatory to establish the relationship between some molecular structures and the resistance phenomena. For example, one the major resistance factor to almost aminoglycoside antibiotics is the amino(6′)-acetyltransferase-Ie/aminoglycoside(2″)-phosphotransferase-Ia [AAC(6=)-Ia/APH(2″)-Ia]. During almost three decades, this bifunctional enzyme structure remained practically unknown. However, the X-ray scattering was the tool to model its structure and the analysis of the impact of substrate binding on the enzyme (Caldwell and Berghuis 2012). The knowledge of the rigid structure, now, could permit the design of more specific therapies able to evade the action of this enzyme or design new molecules that would be able to interfere with the enzyme, letting the aminoglycosides keep their antibacterial activity (Shi and Berghuis 2012; Shi et al. 2013).

The neutron scattering technology can help us to elucidate the secondary side effects of antimicrobial drugs. In a series of experiments conducted in the Institut Laue-Langevin in Grenoble, Barlow and his colleagues from King's College London described by neutron diffraction experiments how the amphotericin B (AmB) interacts with fungal and animal cells membrane. These experiments were the first evidence for the theoretical model of leaky holes resulting from the development of Barrel-like structures, formed in both membranes upon the introduction of AmB. The difference between human and fungal cells was penetration of the barrels at the same AmB concentration, deeper in fungal membranes, explaining in this way, why AmB attack mainly the fungal cells. However, when the dose of drug was increased, the effects reached the animal cells, generating the secondary site effects (Foglia et al. 2012). The atomic details of drug binding have been largely unknown due to the lack of key information on specific hydrogen atom positions and hydrogen binding between the drug and its target enzyme. Acetazolamide (AZM) is a sulphonamide used since a long time ago to treat a wide spectrum of diseases such as glaucoma and epilepsy. When the wrong isomer of AZM is binding to the target enzyme, unpleasant side effects are provoked. The neutron scattering technology gave the precise information about the interactions between carbon anhydrase II and AZM (target enzyme and drug, respectively) (Fisher et al. 2012).

The cell membrane constitutes a significant hydrophobic barrier. This implies the presence of transmembrane proteins responsible to form transmembrane polar pore, to transport the substances in/out. One exception to these carriers is some bacterial toxins, able to insert and cross the lipid bilayer itself. The neutron

scattering helped to study the interaction of colicin N and its outer membrane receptor, the OmpE, that is member of the Omp proteins family, also evolves in the antimicrobial resistance (Clifton et al. 2012). The pH-dependent membrane insertion of the diphtheria toxin T domain in lipid bilayers could be described by specular neutron reflectometry and solid-state NMR spectroscopy (Chenal et al. 2009).

The communication between cells is fundamental in the pluricellular organisms. One part of these interactions is made using vesicles: the vesicles are responsible of the transport of neurotransmitters between nerve cells and also the uptake of glucose from blood in response in insulin signalling. The responsible of mediate in vesicles formation are proteins members of the superfamily protein SNARE. Christie and co-workers used small-angle X-ray scattering (SAXS) and small-angle neutron scattering (SANS) to investigate the interactions between the SNARE—superfamily protein Syntaxin and its regulatory protein Munc18 (Christie et al. 2012).

Other important mechanism of communication between cells is mediated by adhesion proteins, which are the responsible of the formation of intercellular junctions and the control of intermembrane spacing. Neural cell-adhesion molecule (NCAM) is expressed in both developing and adult vertebrate organisms and is a cell surface glycoprotein, which mediates cell adhesion, signalling, migration and plasticity in the central system (Doherty and Walsh 1996). The combination of the neutron and X-ray specular reflectivity helped to elucidate the structure of the ectodomain of NCAM (Clifton et al. 2012).

Cholesterol is an important structural component of most cell membranes, evolved in their organization, dynamics and so on. This lipid is also related in molecular pathways and intracellular cascades (Ikonen 2008; Maxfield and Tabas 2005; Maxfield and Wustner 2002). The healthy cells maintain a cholesterol gradient along the exotic pathways from the endoplasmic reticulum to the plasmatic membrane, suggesting an important role of the homoeostasis of cholesterol in the cells. The importance of cholesterol in the transport is reflected in the severe disorders that its disorder generates, such as the neurodegenerative diseases—Niemann–Pick type-C or Alzheimer's disease. The use of the non-invasive time-resolved small-angle neutron scattering to measure cholesterol intermembrane exchange and intramembrane flipping rate showed a more precise measurement of the transport and the differences with classic techniques, less sensitive and precise (Garg et al. 2011).

There are a huge number of biological applications based in protein arrays based in the interaction between antibodies, scaffold proteins and a surface. The array-based techniques assume the perpendicular disposition of the structure. Polarized neutron reflection was used to probe the perpendicular structure between the IgG, a gold surface and the scaffold protein, concretely a fusion protein based on the porin outer membrane OmpA from *Escherichia coli* and the Z domain of *Staphylococcus aureus* protein A.

2.7 Conclusion

Antimicrobials research faces many challenges regarding the solution of growing threats, even to the collective health and safety. The fight against multiresistant bacterial strains, for instance, implies better knowledge of different molecular processes, new drugs, the development of individualized and preventive clinical approaches, as well as new regimes in drug design and delivery.

Scattering is a very valuable tool for exploring molecular interactions, to further the understanding the mechanisms of different diseases. Development, formulation into effective pharmaceuticals and manufacturing of drugs are fields that can also be very strongly benefited from the scattering techniques.

Apart from the more commercial instruments available, there have been intensive efforts developing big facilities in different countries to provide biologists (and other scientists) with extremely powerful tools to support their investigations. At this moment, more powerful facilities providing a wider range on instruments are planned and will be constructed in the near future. These facilities are providing the ideal environment for multidisciplinary investigations and for pushing forward the frontiers of the scientific knowledge.

This chapter tries to give an overview of the possibilities of using these techniques in the world of antimicrobial research, what opportunities may arise for this discipline by using scattering. From the basic foundations, that give a flavour of the mechanisms involved, to the more suitable instruments for biology and success cases, a comprehensive overview of scattering was provided. The main purpose is to encourage the antimicrobials research community to consider scattering as one of the more powerful experimental alternatives to enhance their investigations.

References

Bauer GS, Fischer WE, Rohrer U, Schryber W (1997) Commissioning of the 1 MW spallation neutron source SINQ. In: Proceedings of the particle accelerator conference, Vancouver, Canada

Bernal JD, Crowfoot D (1934) X-ray photographs of crystalline pepsin. Nature 133:794–795

Borland M, Decker G, Nassiri A, Wait M (2007) Configuration, optics and performance of a 7 GeV energy recovery linac upgrade for the advanced photon source. In: Proceedings of the particle accelerator conference, Alburquerque, NM, USA

Brockhouse BN, Hurst DG (1952) Energy distribution of slow neutrons scattered from solids. Phys Rev 88:542–547

Brockhouse BN, Stewart AT (1955) Scattering of neutrons by phonons in an aluminum single crystal physical. Review 100:756–757

Broome TA (1996) High power targets for spallation sources. In: Proceedings of EPAC 96, Sitges, Spain

Brow BS (1995) News from IPNS. In: Proceedings of the ICANS XIII, Vilingen, Switzerland

Caldwell SJ, Berghuis AM (2012) Small-angle X-ray scattering analysis of the bifunctional antibiotic resistance enzyme aminoglycoside (6') acetyltransferase-ie/aminoglycoside (2') phosphotransferase-ia reveals a rigid solution structure. Antimicrob Agents Chemother 56: 1899–1906

Chadwick J (1932) Possible existence of a neutron. Nature 129:312
Chenal A, Prongidi-Fix L, Perier A, Aisenbrey C, Vernier G, Lambotte S, Haertlein M, Dauvergne MT, Fragneto G, Bechinger B et al (2009) Deciphering membrane insertion of the diphtheria toxin T domain by specular neutron reflectometry and solid-state NMR spectroscopy. J Mol Biol 391:872–883
Christie MP, Whitten AE, King GJ, Hu SH, Jarrott RJ, Chen KE, Duff AP, Callow P, Collins BM, James DE et al (2012) Low-resolution solution structures of Munc18: Syntaxin protein complexes indicate an open binding mode driven by the Syntaxin N-peptide. Proc Natl Acad Sci USA 109:9816–9821
Clifton LA, Johnson CL, Solovyova AS, Callow P, Weiss KL, Ridley H, Le Brun AP, Kinane CJ, Webster JR, Holt SA et al (2012) Low resolution structure and dynamics of a colicin-receptor complex determined by neutron scattering. J. Biol Chem 287:337–346
Cullity BD (1967) Elements of X-ray diffraction
Curbis F, Cutic N, Werin S, Karlberg O, Mak A, Thorin S, Mansten E, Lindau F, Eriksson M (2013) Extension of the MAX IV for a free electron laser in the X-ray region. In: Proceeding of the international particle accelerator conference, Shanghai, China
Danared H (2012) Design of the ESS accelerator. In: Proceedings of the II IPAC, San Sebastian, Spain
Diagnoux AJ, Lander GH (2003). Neutron Data Booklet
Doherty P, Walsh FS (1996) CAM-FGF receptor interactions: a model for axonal growth. Mol Cell Neurosci 8:99–111
Elder FR, Gurewitsch AM, Langmuir RV, Pollock MC (1947) Radiation from electrons in a synchrotron. Phys Rev 71:829–830
Eshraqi M, Danared H (2011) ESS linac, design and beam dynamics. In: Proceedings of the II IPAC, San Sebastian, Spain
Fisher SZ, Aggarwal M, Kovalevsky AY, Silverman DN, McKenna R (2012) Neutron diffraction of acetazolamide-bound human carbonic anhydrase II reveals atomic details of drug binding. J Am Chem Soc 134:14726–14729
Foglia F, Lawrence MJ, Demee B, Fragneto G, Barlow D (2012) Neutron diffraction studies of the interaction between amphotericin B and lipid-sterol model membranes. Sci Rep 2:778
Friedrich W, Knipping P, Laue M (1912) Interferenz-Erscheinungen bei Röntgenstrahlen. Sitzungsber Kgl Bayrischen Akad Wiss 1:303–322
Gardner ISK (1994) ISIS status report. In: Proceedings of the EPAC, 94, London, England
Garg S, Porcar L, Woodka AC, Butler PD, Perez-Salas U (2011) Noninvasive neutron scattering measurements reveal slower cholesterol transport in model lipid membranes. Biophys J 101:370–377
Garnett RW, Rybarcyk LJ, Rees DE, Tajima T, Pitchet EJ (2011) High power options for LANSCE. In: Proceedings of the particle accelerator conference, New York, USA
Gidalevitz D, Ishitsuka Y, Muresan AS, Konovalov O, Waring AJ, Lehrer RI, Lee KY (2003) Interaction of antimicrobial peptide protegrin with biomembranes. Proc Natl Acad Sci USA 100:6302–6307
Gottfried K, Yan TM (2003) Quantum mechanics: fundamentals
Goward FK, Barnes DE (1946) Experimental 8 MeV synchrotron for electron acceleration. Nature 158:413
Guinier A, Fournet G (1955) Small-angle scattering of X-rays
Havighurst RJ (1927) Electron distribution in the atoms of crystals. Sodium chloride, and lithium, sodium and calcium fluoride. Physical. Review 29:1
He K, Ludtke SJ, Huang HW, Worcester DL (1995) Antimicrobial peptide pores in membranes detected by neutron in-plane scattering. Biochemistry 34:15614–15618
He K, Ludtke SJ, Worcester DL, Huang HW (1996) Neutron scattering in the plane of membranes: structure of alamethicin pores. Biophys J 70:2659–2666
Ikonen E (2008) Cellular cholesterol trafficking and compartmentalization. Nat Rev Mol Cell Biol 9:125–138

Kendrew JC, Bodo G, Dintzis HM, Parrish RG, Wyckoff H, Phillips DC (1958) A three-dimensional model of the myoglobin molecule obtained by x-ray analysis. Nature 181:662–666

Latal A, Degovics G, Epand RF, Epand RM, Lohner K (1997) Structural aspects of the interaction of peptidyl-glycylleucine-carboxyamide, a highly potent antimicrobial peptide from frog skin, with lipids. European J Biochem/FEBS 248:938–946

Liang L, Rinaldi R, Schober H (2009) Neutron applications in earth, energy and environmental sciences. Neutron scattering applications and techniques. Lightsources.

Lohner K, Prenner EJ (1999) Differential scanning calorimetry and X-ray diffraction studies of the specificity of the interaction of antimicrobial peptides with membrane-mimetic systems. Biochim Biophys Acta 1462:141–156

Ludtke SJ, He K, Heller WT, Harroun TA, Yang L, Huang HW (1996) Membrane pores induced by magainin. Biochemistry 35:13723–13728

MacMillan EM (1945) The synchrotron—a proposed high energy accelerator. Phys Rev 68:143

Maxfield FR, Tabas I (2005) Role of cholesterol and lipid organization in disease. Nature 438:612–621

Maxfield FR, Wustner D (2002) Intracellular cholesterol transport. J Clin Investig 110:891–898

Neville F, Hodges CS, Liu C, Konovalov O, Gidalevitz D (2006) In situ characterization of lipid A interaction with antimicrobial peptides using surface X-ray scattering. Biochim Biophys Acta 1758:232–240

Oliphant MO (1943) The acceleration of particles to very high energies. Classified memo submitted to DSIR University of Birmingham Archive

Peggs, S. (2013). ESS technical design report (ESS-2013-001)

Pieper J, Buchsteiner A, Dencher NA, Lechner RE, Hauss T (2008) Transient protein softening during the working cycle of a molecular machine. Phys Rev Lett 100:228103

Plum (2010) Status of the SNS power ramp up. In: Proceedings of the I IPAC, Kyoto, Japan

Revol JL, Biasci JC, Bouteille JF, Ewald F, Farvacque L, Franchi A, Gautier G, Goirand L, Hahn M, Hardy L et al. (2013) ESRF operation and upgrade status. In: Proceedings of the international particle accelerator conference, Shanghai, China

Rutherford E (1920) Bakerian lecturer. nuclear constitution of atoms. In: Proceedings of the royal society a: mathematical, physical and engineering sciences, vol 97, p 374

Shi K, Berghuis AM (2012) Structural basis for dual nucleotide selectivity of aminoglycoside 2'-phosphotransferase IVa provides insight on determinants of nucleotide specificity of aminoglycoside kinases. J Biol Chem 287:13094–13102

Shi K, Caldwell SJ, Fong DH, Berghuis AM (2013) Prospects for circumventing aminoglycoside kinase mediated antibiotic resistance. Frontiers Cell Infect Microbiol 3, doi 10.3389/fcimb.2013.00022

Squires GL (2012) Introduction to the theory of thermal neutron scattering

Suller VP (2002) Status of the diamond light source project. In: Proceedings of European particle conference, Paris, France

Tardieu A, Luzzati V, Reman FC (1973) Structure and polymorphism of the hydrocarbon chains of lipids: a study of lecithin-water phases. J Mol Biol 75:711–733

van Hove L (1954) Correlations in space and time and Born approximation scattering in system of interacting particles. Phys Rev 95:249–262

Veksler VI (1944) A new method of accelerating relativistic particles. Comptes Rendus (Dokaldy) de l'Academie de Sciencies de l'URSS 43:8

Warren BE (1969) X-ray diffraction

White M (2002) The spallation neutron source (SNS). In: Proceedings of LINAC, Gyeongju, Korea

Wood K, Plazanet M, Gabel F, Kessler B, Oesterhelt D, Tobias DJ, Zaccai G, Weik M (2007) Coupling of protein and hydration-water dynamics in biological membranes. Proc Natl Acad Sci USA 104:18049–18054

http://www.springer.com/978-3-642-40443-6

Antimicrobial Compounds
Current Strategies and New Alternatives
González Villa, T.; Veiga-Crespo, P. (Eds.)
2014, XVI, 316 p. 47 illus., 18 illus. in color., Hardcover
ISBN: 978-3-642-40443-6